Spectral, crystal structure of novel Pyran-2-one Zwitterion Schiff derivative: Thermal, Physicochemical, DFT/HSA-interactions, enol↔imine tautomerization and anticancer activity

Article *in* Journal of Molecular Structure · April 2024

DOI: 10.1016/j.molstruc.2024.138258

12 authors, including:

Tabti Salima
Université Mohamed El Bachir El Ibrahimi de Bordj Bou Arréridj
16 PUBLICATIONS **183** CITATIONS
SEE PROFILE

Djouhra Aggoun
45 PUBLICATIONS **464** CITATIONS
SEE PROFILE

Diaa Aref
An-Najah National University
12 PUBLICATIONS **133** CITATIONS
SEE PROFILE

Ashraf Sawafta
An-Najah National University
18 PUBLICATIONS **127** CITATIONS
SEE PROFILE

Journal of Molecular Structure 1310 (2024) 138258

Contents lists available at ScienceDirect

Journal of Molecular Structure

journal homepage: www.elsevier.com/locate/molstr

Spectral, crystal structure of novel Pyran-2-one Zwitterion Schiff derivative: Thermal, Physicochemical, DFT/HSA-interactions, enol↔imine tautomerization and anticancer activity

Salima Tabti [a,b,*], Djouhra Aggoun [c], Diaa Aref [d], Ashraf Sawafta [e], Amel Djedouani [f], Ahmed Abu-Rayyan [g], Abeer AlObaid [h], Jerome Lhoste [i], Carine Robert [j], Sandy Augste [i], Khalil Shalalin [k], Ismail Warad [d,*]

[a] Department of Ecology and Environment, Faculty of Life and Natural Sciences of Earth and Universe Sciences, University Mohamed El Bachir El Ibrahimi of Bordj Bou Arreridj, 34000, Algeria
[b] Laboratory of Electrochemistry and Environment, University Mohamed El Bachir El Ibrahimi of Bordj Bou Arreridj, 34000, Algeria
[c] Laboratory of Electrochemistry, Molecular Engineering and Catalysis Redox (LEIMCR), Department of Engineering Sciences, Faculty of Technology, Farhat ABBAS University Setif-1, Algeria
[d] Department of Chemistry, Science College, An-Najah National University, Nablus P.O. Box 7, Palestine
[e] Biology and Biotechnology Department, An-Najah National University, P.O. Box 7, Nablus, Palestine
[f] Superior School of Constantine, University City Ali Mendjeli, 25000 Constantine, Algeria
[g] Chemistry Department, Faculty of Arts & Science, Applied Science Private University, P.O. Box 166, Amman 11931, Jordan
[h] Department of Chemistry, College of Science, King Saud University, P.O. Box 2455, Riyadh 11451, Saudi Arabia
[i] Institute of Molecules and Materials of Le Mans (IMMM)-UMR 6283 CNRS, Le Mans University, Avenue Olivier Messiaen, 72085, Le Mans Cedex 9, France
[j] Institute of Research Chemistry Paris, CNRS, Chemistry ParisTech, PSL University, 75005 Paris, France
[k] Department of Dentistry and Dental Surgery, Faculty of Medicine and Health Sciences, An-Najah National University, P.O. Box 7, Nablus, Palestine

ARTICLE INFO

Keywords:
Schiff base
Zwitterionic
Enol↔imine tautomerism
XRD/HSA
DFT
Anticancer

ABSTRACT

A novel Schiff base (SB) derivative, (E)-3-(1-((2,6-diisopropylphenyl)-imino)-ethyl)-4-hydroxy-6-methyl-2H-pyran-2-one, was synthesized in a high yield through the direct condensation of 2,6-diisopropylaniline with 3-acetyl-4-hydroxy-6-methyl-2H-pyran-2-one in ethanol under reflux conditions. The synthesized ligand was identified using different elemental analysis (CHN-EA) and spectroscopic techniques (2D-nuclear magnetic resonance (^{1}H- & ^{13}C- NMR), Fourier transform infrared (FT-IR) and mass (MS) spectroscopies), and their structural analysis was performed by single crystal X-ray diffraction (XRD). In addition, the thermogravimetric behavior of the ligand was evaluated using thermogravimetric analysis (TGA) and differential thermal analysis (DTA). The DFT calculations on the gaseous state and in chloroform as solvent using B3LYP-D3/6–311++*G*(2d, p) and the HSA calculations were performed to examine the stability of the tautomeric forms of the ligand and to understand its Zwitterionic behaviors. The results showed that the ligand exhibits a zwitterionic form stabilized by an intramolecular single proton transfer process between the enol and imine tautomerism. The enol↔imine tautomerization was determined by XRD and computed by DFT/HSA calculations, which proved the stabilization of the [N^{+} – – H···O^{--}] zwitterionic form via S6 intra-H-bond. In addition, the Colorimetric [3-(4,5-dimethylthiazol-2-yl)-2,5-diphenyltetrazolium bromide (MTT) assay showed that the ligand exhibits high activity against cancer cells, specifically HeLa cells, at low concentrations.

1. Introduction

Zwitterion SB with iminium and hydroxyl units broadens their range of properties and expands the classical Schiff bases' biological and industrial applications [1,2]. In general, SB and the Zwitterion of SB have been critical in the preparation of many types of metallic complexes via the poly-chelated mode of coordination using all of the ionic metal centers, resulting a unique 3D-structures and very stable complexes with different stereochemical geometries [1,2].

Tautomerization is a common phenomenon in such compounds;

* Corresponding authors.
E-mail address: warad@najah.edu (I. Warad).

https://doi.org/10.1016/j.molstruc.2024.138258
Received 3 December 2022; Received in revised form 28 March 2024; Accepted 4 April 2024
Available online 6 April 2024

various types of tautomerization regarding atomic exchange within a molecular structure have been reported [2]. Among these atomic exchanges is the transfer of the hydrogen atom between nitrogen and oxygen of keto-amine and enol-imine tautomer, which is extremely important in many fields of science and medicine [1–6], including molecular biology, pharmacology, and organic and medicinal chemistry [3–5]. However, studying tautomerization is a challenge that requires cooperation among chemistry and molecular biology since most tautomeric processes are difficult to observe due to their structural fast exchange with low thermodynamic energy [1]. As a result, analyzing the energetic and structural parameters caused by hydrogen atom exchange between the tautomeric forms would be critical to understanding the molecular kinetic behavior and chemical properties, which would aid in the future development and design of novel SB ligands and their metal complexes with their new potential clinical and pharmaceutical applications [6,7].

This manuscript aims to synthesize a brand-new zwitterionic polychelate SB ligand derived from the chemical hydroxyl-pyran-2-one. This ligand's spectral, structural, and putative biological actions have received the majority of the research attention [8–13]. SC-XRD was used to determine the structure of the Zwitterionic SB ligand; this was followed by NMR (^{1}H and ^{13}C), elemental analysis (CHN-EA), mass spectroscopy, TG/DTG, and infrared spectra to provide additional support. The interactions were calculated using XRD/HSA, MO/MEP/MAC/NBA analyses, and DFT calculations for the [O—H···N] single proton intra-migration mechanism that leads to enol-imine tautomerization. The anti-cancer properties and thermal behavior were assessed.

2. Experimental

2.1. Materials and measurements

All chemicals were obtained from Across Company and used without further purification.

The ^{1}H NMR was performed on a Jeol GSX WB spectrometer at 270 MHz using $CDCl_3$ solvent. Solid-state FT-IR was performed on a Shimadzu FTIR-8010 M spectrometer in range of 4000–400 cm^{-1}. The Mass spectrum we have employed a GC (ITQ 1100) and LC (Agilent 1290 Infinity II) coupled with ionic tramp detector (Agilent 6470 Triple Quad LC/MS).

2.2. Synthesis of desired ligand

The synthesis of the desired Schiff base ligand was carried out by using 1 mmol of dehydroacetic acid and 1 mmol of 2,6-di isopropyl aniline then 10 ml ethanolic solution was added in the presence of few granules of molecular sieve. The resulting solution was refluxed for 72 h and the reaction was monitored by TLC (CH_2Cl_2/ ethanol, 9.7/0.3). After that, the solution was filtrated and the resulting gold color solid was watched with diethyl ether. The crystals are obtained after slow evaporation in CH_2Cl_2. Finally, the ligand was obtained, being the yield (72%, 2.37 g), m.p.=165 °C.

^{1}H NMR (300 MHz, $CDCl_3$), δ (ppm): δ 1.22 (12H, 4CH_3, d, J = 7.0 Hz), 2.1 (3H, CH_3, s), 2.2 (3H, CH_3, s), 2.8 (2H, 2CH, M), 5.8 (1H, CH, s), 7.1–7.3 (3H, pH, m), 15.2 (1H, OH, s). **^{13}C NMR** (300 MHz, $CDCl_3$), δ(ppm): δ 20.0 (1C, s), 22.6 (1C, s), 24.1 (4C, s), 28.7 (2C, s), 96.7 (1C, s), 107.6 (2C, s), 124.3 (1C, s), 129.2 (1C, s), 131.7 (1C, s), 144.4 (2C, s), 163.6 (1C, s), 177.1 (1C, s), 185.1 (1C, s). Selected IR bands (KBr pellet, cm^{-1}): 2960 (C_{Ph}-H), 2900–2850 (C_{aliph}-H), 1713 (C = O), 1650 (O = C—O), 1622 (C = N), 1502 (C = C), 1350 (C—N), 1021(C—O-C)$_{pyran}$, 1010–750 (C—H)$_{bending}$.

2.3. Computational and XRD-analysis details

Gaussian 09 W 32-bit software was utilized for all DFT operations in the gaseous state at DFT/B3LYP method and 6–311++G(d,p) as the basis set [14]. The HSA was carried out using Crystal Explorer 3.1 [15].

Crystals were selected under a polarizing optical microscope and mounted on Micro Mount needles (MiTiGen) for single-crystal X-ray diffraction experiments. X-ray intensity data were collected at room temperature on a Bruker APEX II Quazar diffractometer (4 circle Kappa goniometer, CCD detector) using an Imsmicrofocus source (Mo-K_α radiation with λ = 0.71073 Å).

The structure solutions were obtained by direct methods, developed by successive difference Fourier syntheses, and refined by full-matrix least squares on all F_2 data using SHELX program suite in Bruker APEX2 interface [16,17]. The structure solutions were obtained by direct methods, developed by successive difference Fourier syntheses, and refined by full-matrix least-squares on all F^2 data using SHELX program suite in Bruker APEX2 interface [18,19]. Details of the structure determinations are given in Table 1.

Table 1
Refinement details of the solved crystal structure.

Chemical formula	$C_{20}H_{25}NO_3$
CCDC	2,336,259
Formula weight	327.41 g/mol
Temperature	296(2) K
Wavelength	0.71073 Å
Crystal size	0.144 x 0.474 x 0.508 mm
Crystal system and Space group	Triclinic P −1
Unit cell dimensions	a = 8.3759(18) Å α = 79.078 (11)°
	b = 9.9587(16) Å β = 86.822 (13)°
	c = 11.469(2) Å γ = 77.396(11)°
Volume	916.6(4) $Å^3$
Z	2
Density (calculated)	1.189 g/cm^3
Absorption coefficient	0.079 mm^{-1}
F(000)	352
Theta range for data collection	2.49 to 27.50°
Index ranges	−10<=h<=10, −12<=k<=12, −14<=l<=14
Reflections collected	10,905
Independent reflections	4154 [R(int) = 0.0582]
Coverage of independent reflections collected	99.1 % 10,905
Absorption correction	Multi-Scan
Refinement method	Full-matrix least-squares on F^2
Function minimized	$\Sigma\, w(F_o^2 - F_c^2)^2$
Data / restraints / parameters	4154 / 0 / 223
Goodness-of-fit on F^2	1.024
Δ/σ_{max}	0.002
Weighting scheme	$w = 1/[\sigma^2(F_o^2)+(0.0769P)^2 +$ 0.0183P] where $P=(F_o^2+2F_c^2)/3$
Final R indices	data; $I > 2\sigma(I)$,R1 = 0.0619, wR2 = 0.1519
Largest diff. peak and hole	0.166 and −0.171 eÅ^{-3}
R.M.S. deviation from mean	0.038 eÅ^{-3}

2.4. Cell lines

Solutions of the newly prepared compound were prepared at a concentration of 1 mg per 1 mL of DMSO solvent and then incubated at 4 °C, several concentrations of (500, 250, 125, 62.5, and 32.25 μg/ml) were then made available via the serial dilution method.

Human cervix cancer cells (ATCC number: CCL-2, from a cervical carcinoma), and normal muscle cells (L6, ATCC number: CRL-1458, human, from the skeletal muscle) were grown in RPMI medium supplemented with 10 % fetal calf serum, 1 % non-essential amino acid, 1 % l-glutamine, 1 % penicillin-streptomycin and 1 % amphotericin B. Both cell lines were grown in a humidified atmosphere of 95 % air, and 5 % CO_2 at 37 °C, the culture medium was changed at least twice a week as needed. All chemicals used were purchased from Biological Industries except for the amphotericin B and MTT reagent from SIGMA Company. Cell lines were purchased from ATTC. Cells (2 × 10^4 cells/well) with

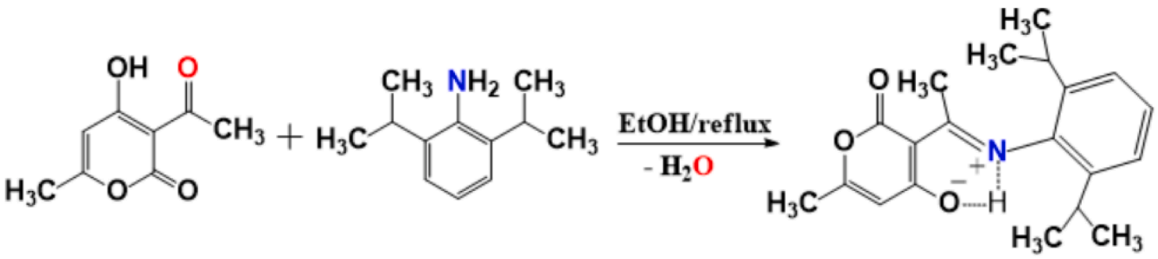

Scheme 1. Preparation of the desired Zwitterion Schiff base.

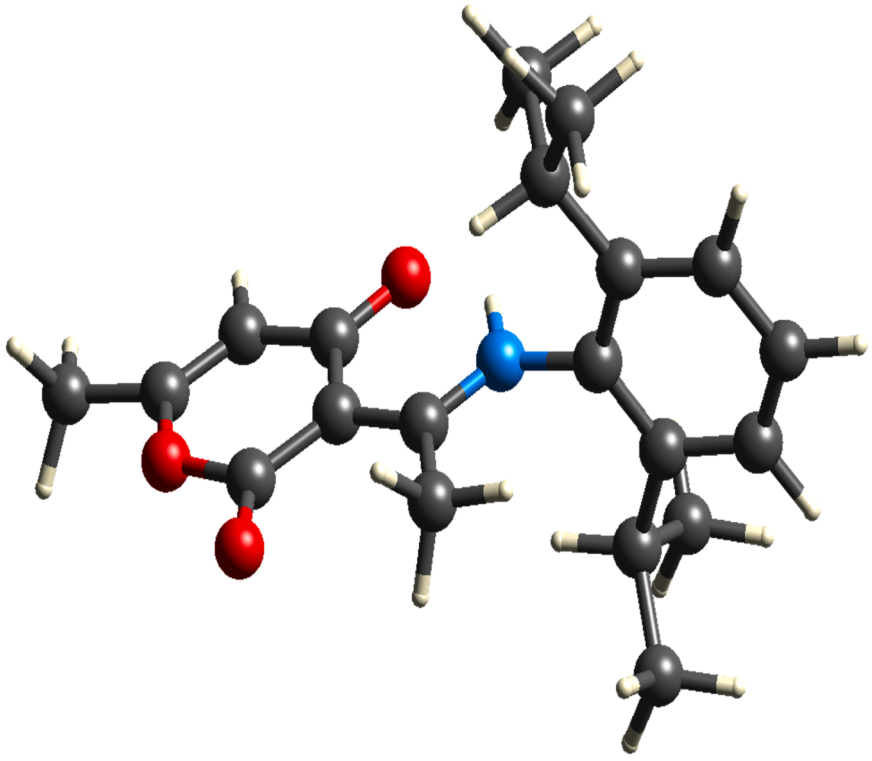

Fig. 1. ORTEP picture of $C_{20}H_{25}NO_3$.

40–50 % confluence were seeded on a 96-well plate, the cells were then treated with the different concentrations.

2.5. Calorimetric MTT assay

The anticancer effect of the new compound against HeLa cells and L6 cells was estimated by the 3-[4,5-dimethylthiazole-2-yl]−2, 5-diphenyl-tetrazolium bromide (MTT) assay using (cell growth determination kit MTT based, Sigma). Cells (2×10^4 cells/well) were incubated with various concentrations of the compounds (500, 250, 125, 62.5, and 32.25 μg /ml) in 5 % CO_2, 95 % air, and 100 % relative humidity at 37 °C for 24 h in an FBS-free medium. Aseptically MTT solution was added in an amount equal to 10 % of the culture volume. Then cultures were returned to the incubator and incubated for 4 h. After the incubation period, the resulting MTT formazan crystals were dissolved by the addition of MTT solvent in an amount equal to the original culture volume. The addition of MTT solvent was performed after the removal and disposal of the culture fluid as HeLa cells were still attached to the culture surface. The absorbance at 570 nm was measured using a microplate reader (Labtech, UK). The relative cell viability was determined by the amount of MTT converted to the insoluble formazan salt. The data are expressed as the mean percentage of viable cells as compared to the respective control.

3. Results and discussion

3.1. Preparation and characterization of the prepared Zwitterionic Schiff base ligand

The (E)−3-(1-((2,6-diisopropylphenyl)imino)ethyl)−4-hydroxy-6-methyl-2H-pyran-2-one (the desired zwitterionic Schiff base) was synthesized by mixing equimolar amounts of 2,6-diisopropylaniline and 3-acetyl-4-hydroxy-6-methyl-2H-pyran-2-one in ethanol and conducting condensation under reflux conditions, as shown in Scheme 1. This process resulted in a 72 % yield of solid products.

3.2. XRD characterization supported by DFT calculations

The 3D structure of the solid ligand was determined using XRD analysis, revealing it to be in the keto form rather than the expected enol form. The zwitterionic salt compound was formed through enol-keto tautomerization, which was proposed by DFT studies in the gaseous state using B3LYP-D3/6–311++*G*(2d,p) level of theory [13].

The ORTEP picture and DFT-optimized geometry of the desired Zwitterionic Schiff base have been presented in Fig. 1 and Fig. 2, respectively. These figures and Table 2 present all the structure parameters of the molecule. The DFT and XRD structural analysis

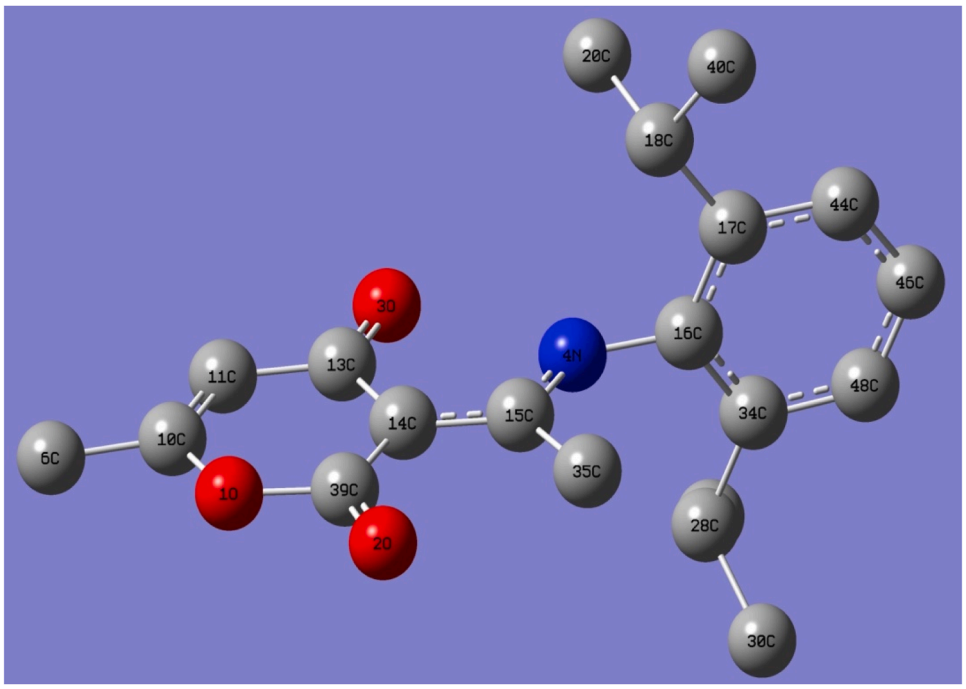

Fig. 2. DFT-optimized structure of $C_{20}H_{25}NO_3$.

Table 2
All the angles (°) and bond distances (Å) for desired ligand.

No.	Bond		XRD	DFT	No.	Angle			XRD	DFT
1	O1	C2	1.3605	1.3574	1	C2	O1	C16	122.6	122.93
2	O1	C16	1.3954	1.4092	2	C6	N1	C7	128	128.18
3	O2	C16	1.2043	1.2141	3	O1	C2	C1	111.43	111.59
4	O3	C4	1.2473	1.2569	4	O1	C2	C3	121.54	122.25
5	N1	C6	1.3099	1.3365	5	C1	C2	C3	127.02	126.16
6	N1	C7	1.4474	1.4377	6	C2	C3	C4	121.64	121.14
7	C1	C2	1.4903	1.4954	7	O3	C4	C3	120.03	119.7
8	C2	C3	1.3145	1.3476	8	O3	C4	C5	122.77	123.68
9	C3	C4	1.4414	1.4524	9	C3	C4	C5	117.2	116.62
10	C4	C5	1.4353	1.4624	10	C4	C5	C6	120.52	120.7
11	C5	C6	1.4229	1.4224	11	C4	C5	C16	119.51	120.15
12	C5	C16	1.435	1.4525	12	C6	C5	C16	119.97	119.15
13	C6	C15	1.4886	1.5034	13	N1	C6	C5	118.97	118.42
14	C7	C8	1.3967	1.4138	14	N1	C6	C15	117.68	118.31
15	C7	C14	1.3875	1.4087	15	C5	C6	C15	123.35	123.27
16	C8	C9	1.5228	1.5278	16	N1	C7	C8	118.43	118.51
17	C8	C18	1.389	1.3986	17	N1	C7	C14	117.95	119.15
18	C9	C10	1.5205	1.5445	18	C8	C7	C14	123.45	122.21
19	C9	C17	1.5328	1.5373	19	C7	C8	C9	121.51	120.93
20	C11	C12	1.5322	1.5417	20	C7	C8	C18	116.42	117.63
21	C12	C13	1.5059	1.5408	21	C9	C8	C18	122.07	121.41
22	C12	C14	1.5149	1.5254	22	C8	C9	C10	111.06	110.83
23	C14	C20	1.3923	1.4017	23	C8	C9	C17	113.52	113.66
24	C18	C19	1.3713	1.3941	24	C10	C9	C17	110.48	110.44
25	C19	C20	1.3685	1.39	25	C11	C12	C13	111.12	111.05
					26	C11	C12	C14	110.58	111.22
					29	C13	C12	C14	112.47	111.91
					30	C7	C14	C12	122.68	122.36
					31	C7	C14	C20	117.08	117.77
					32	C12	C14	C20	120.23	119.87
					33	O1	C16	O2	113.74	114.73
					34	O1	C16	C5	117.32	116.91
					35	O2	C16	C5	128.92	128.36
					36	C8	C18	C19	121.55	121.15
					37	C18	C19	C20	120.47	120.15
					38	C14	C20	C19	120.99	121.09

confirmed the stability of the zwitterionic ionic molecule, with the proton of the enol attracted by the imine functional group to form an [N^+–H···O^-] intra-H-bond linking the hydroxyl and iminium groups, as seen in other previously published zwitterionic structures [20,21]. The bond distances indicated a C—N iminium distance of 1.308(3) Å, which is consistent with related compounds [22,23]. This distance is slightly

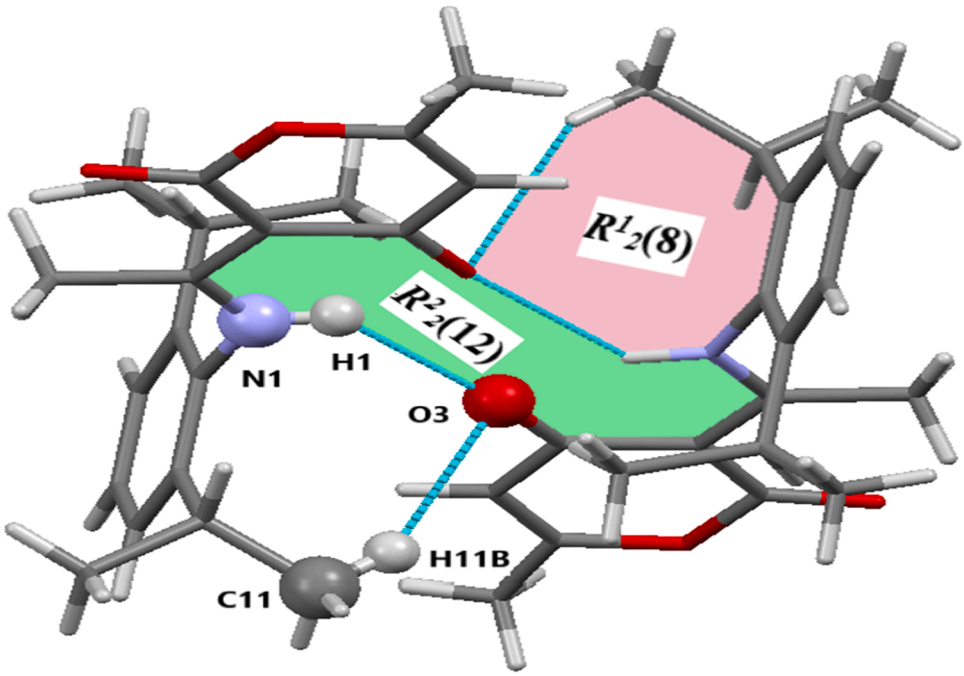

Fig. 3. $R_2^2(12)$ and $R_2^1(8)$ rings motif.

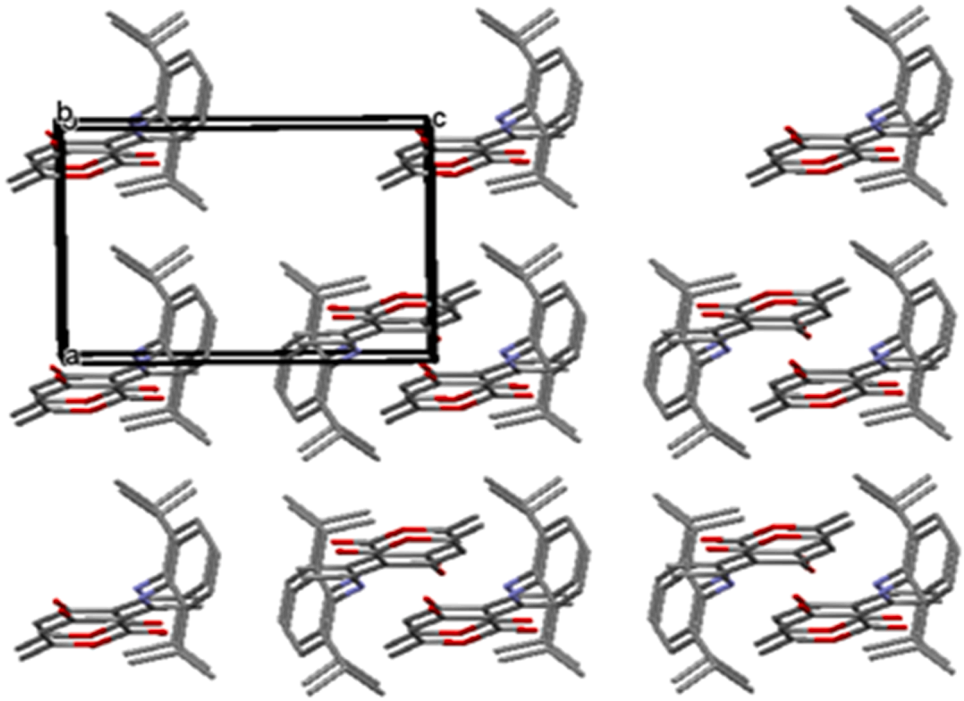

Fig. 4. Packing arrangement along the (ac) plane.

longer than the typical C = N bond distance (1.269 Å) [24], and shorter than the C—N single bond distance (1.409 Å) [25]. This observation can be attributed to the formation of a [C = O···H–N] intra-H-bond and its resonance. The bond length of C—$O_{Hydroxy}$ was found to be 1.249(3) Å, which falls between the single and double O to C bond lengths (1.222 Å and 1.362 Å, respectively) [26]. The C—C bonds linked to the iminium and enol functional groups have intermediate lengths between double and single bonds, supporting the delocalization of π electrons over the bonds between the enol-iminium unit. The DFT stereo-calculation showed a high degree of agreement with the XRD-determined real structure, as the keto isomer is more stable than the enol isomer. The conversion from the enol form to the carbonyl form, rather than the hydroxyl form, has led to the proton being pushed towards the iminium functional group, forming the [N^+–H···O^-] intra-H-bond zwitterionic ionic form.

In the crystal lattice, molecules are aligned in columns parallel to the [0 0 1] axis and arranged head to foot along the c axis. The stability of the lattice is not solely due to N1–H1···O3 H-bonds, but also other non-classical C11–H11b···O3 H-bonds that result in the formation of $R_2^2(12)$ and $R_2^1(8)$ rings motif (Fig. 3) and layers that extend parallel to the (ab)

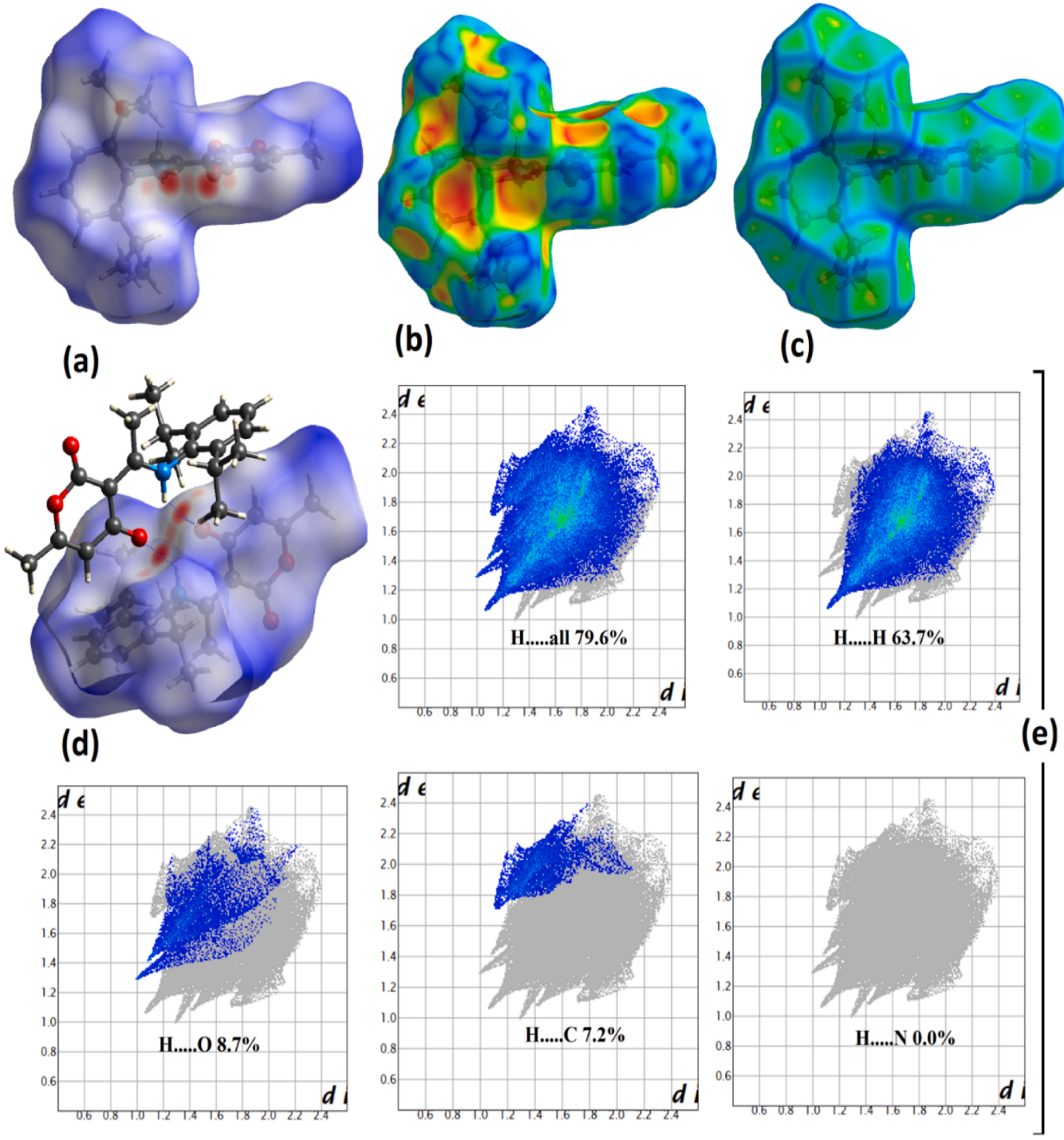

Fig. 5. (a) d_{norm}, (b) shape index, (c) crudeness, (d) molecule-molecule interactions and (d) atom-atom 2D-FB plots.

plane (Fig. 4).

The 3D-structural parameters of DFT optimized structure were compared to the experimental collected XRD results. DFT and XRD bond length data are with a high agreement with graphical correlation $R^2 = 0.984$, similarly the relation of the angles also reflected a significant matching with $R^2 = 0.987$. In contrast to that, the dihedral angles values of the DFT and XRD did not show a sufficient degree of stereochemistry compatibility.

3.3. HSA/2D-FP computations

The HSA/2D-FP analyses were conducted on the original crystal CIF file. The strength of the interactions, such as H-bonds, were depicted as red spots of different sizes on the surface of the ligand molecule [27–32]. Since the desired compound is with 3O and 1 N as polar heteroatoms, many red spots via d_{norm} were disclosed on the surface of the ligand molecule **(**Fig. 5**a-c)**, and the largest red spot was found around the oxygen of the ket/enol part is indicating for the formation of an intra-molecular [N^{+}–H···O^{-}] H-bond. Other big red spots were also observed around the O atom of ester and the C = O of ketone, indicating

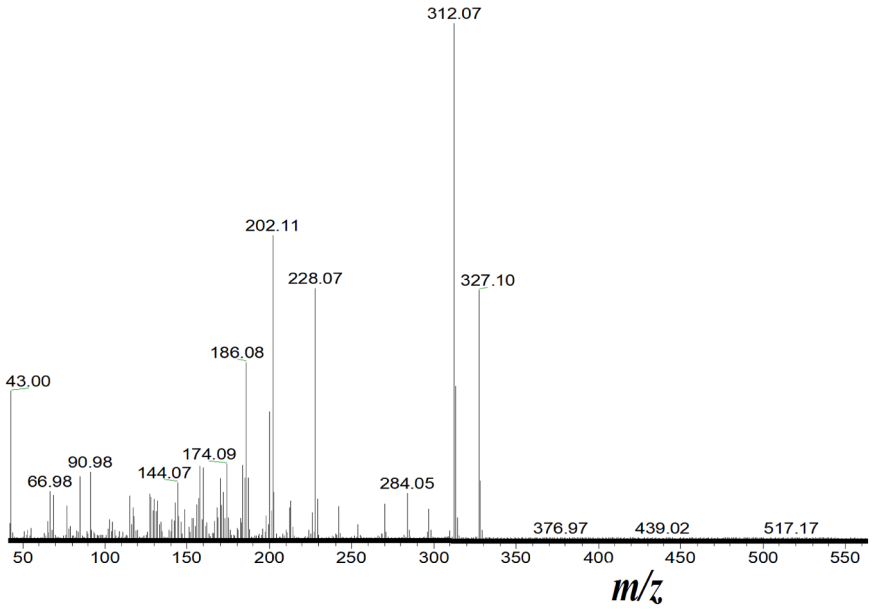

Fig. 6. GCEI-MS of the desired ligand.

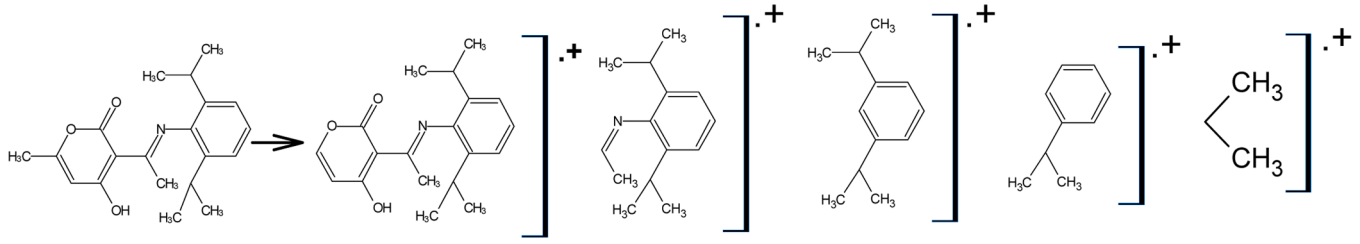

Scheme 2. Proposed major fragments ions deduced from the mass spectra of ligand.

the presence of [C–H···O] non-classical H-bonds (Fig. 5d). The 2D-FP calculations revealed the intermolecular interaction strengths in the following order: H···H(63.7)>*O*···H(8.7)>C···H(7.2)>*N*···H(0). Moreover, nitrogen has no H-bonding with the surrounding protons as can be seen in Fig. 5e, the intermolecular interaction contributions are equal to zero, such seen supported that it carries a positive charge preventing it from connecting with any neighboring protons, while the oxygen atoms are active in such interactions. These findings are in good agreement with the previous crystallographic XRD observations.

3.4. CHN, GCEI, NMR and FT-IR characterization

The atomic continents of the prepared Zwitterion Schiff base ligand were determined by (CHN-EN) elemental analysis, which showed measured values of C (73.21 %), H (7.58 %), and N (4.32 %) and theoretical values of C (73.37 %), H (7.70 %), and N (4.28 %). The molecular weight was also confirmed by mass spectrometry (GCEI) with a measured value of 327.06 Da (theoretical value of 327.8 Da), as seen in Fig. 6, verifying the formula of $C_{20}H_{25}NO_3$. The molecular structure deduced from mass fragmentation patterns is included in the (Scheme 2). A base peak with *m/z* equal to 312.02 was observed assigned to the mass of $[SB\text{-}CH_3]^+$ ion. Moreover, another important fragment with *m/z* = 202.04 is also observed, which may correspond to the fragmentation of $[C_5H_2O_3-]^+$ ion, On the other band a fragment at 158.03 was assigned to the fragmentation of $[CH_3-C{=}N-]^+$ion. The fragment with *m/z* = 114.97 was assigned to the fragmentation of isopropyl and for the last one at 42.97 is assigned to the fragmentation of phenyl.

The ^{1}H NMR using $CDCl_3$ solvent was served to jug the enol-keto structural formula favored isomer of the desired ligand in liquid (Fig. 7a). For instance, the peak at very high chemical shift = 15.4 ppm can be assigned to O–H (1H) and not to N—H [13], such observations strongly supported the tendency of the compound toward enolate form instead of keto one in the liquid state. The protons of the compound were detected on their expected chemical shifts, and phenylic protons are detected as two multiplet groups with δ_H in 7.0–7.6 ppm (3H) range. The proton of the vinylic functional group was cited as an expected singlet (1H) at 5.7 ppm. The 4-methyls of isopropyl are verified at 1.3 ppm as a doublet (12H), methyl of C = N was cited at 2.1 ppm (3H), and methyl of C = C was cited at 2.8 ppm (3H).

The theoretical ^{1}H NMR measurements based on the DFT exhibited a significant level of agreement with the experimental results, as depicted in Fig. 7b. Except for the hydroxyl proton, which showed a high chemical shift deviation from the experimental measurement with a value of 13.3 ppm instead of the exp. expected 15.4 ppm, with $\Delta\delta_H = 2.1$ ppm. On other hand, it can be concluded that all other DFT-^{1}H NMR protons chemical shifts closely matched the practical values, with deviations values not exceeding $\Delta\delta_H = 0.6$ ppm in the highest cases. The examination of the comparison between Exp./DFT ^{1}H NMR involved considering two main metrics: root mean square deviation (RMSD) and coefficient of determination (R^2). The values obtained for these metrics were 0.8375 and 0.9875 respectively (Fig. 7c and Table 3).

As expected, the ^{13}C NMR spectra showed the presence of two carbon groups, the first is aliphatic with a low chemical shift and the other is an aromatic and unsaturated functional group with a higher chemical shift. With the help of chemical shift values, each sign belongs to which carbon atom as seen in Fig. 8a. The carbons of the desired Schiff base were recorded in δ_C 20–185 ppm range, the sp^3, sp^2-phen, C = N and C = O C-types were recorded experimentally to their expected chemical shifts as

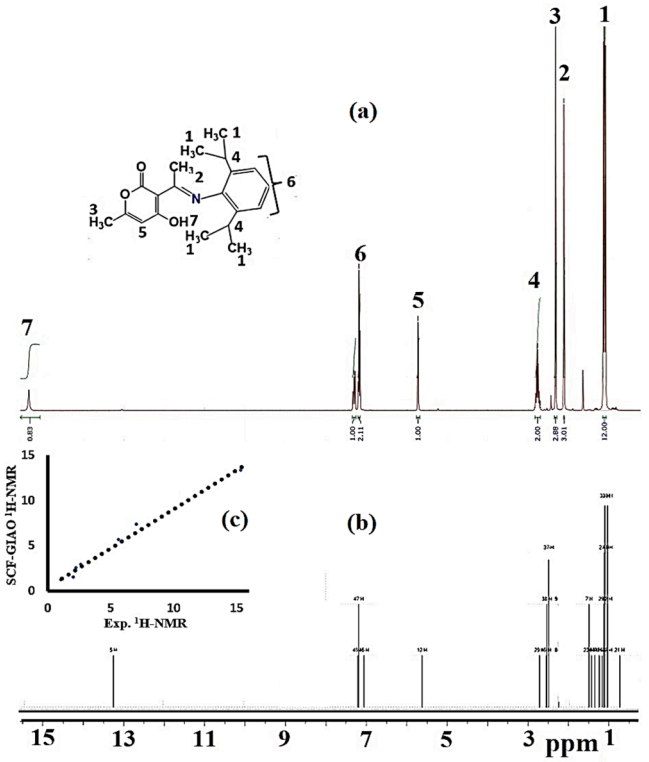

Fig. 7. ^{1}H NMR of the desired ligand: (a)Exp., b) DFT, and (c)Exp/DFT correlation.

recorded directly in Fig. 4c1. The carbon atoms of the target Schiff base were measured within the δ_C range of 20–185 ppm. The experimental recording of the sp^3, sp^2-Aromatic, C = N, and C = O carbon types indicated their expected chemical changes, as depicted in Fig. 8b. The theoretical SCF-GIAO ^{13}C NMR observations demonstrated a notable degree of concurrence with the experimental findings (Fig. 8b), The compounds C 13 and 6 exhibited the greatest deviation in chemical shift, with δ_C values of 16.6 and 13.4 ppm, respectively. The chemical shifts of all the other DFT-^{13}C NMR carbons closely corresponded to their experimental values. The comparison between Exp./DFT ^{13}C NMR was examined, revealing a significant level of competitiveness, since the R^2 and RMSD values were found to be 0.9888 and 5.7026, respectively (see Fig. 8c and Table 3).

The FT-IR spectrum (shown in Fig. 9a) of the synthesized ligand was recorded in the solid state, the absent of band at 3500–3300 cm^{-1} supported the existence of intramolecular H-bonds due to enol-imine [*N*+—H…$^{-}$*O*] zwitterionic in solid state, since intra-H-bond can't be detected by FT-IR, and only the SC-XRD-analysis can confirm it. Therefore, the solid-state FT-IR spectrum verifies the keto form, since it was stabilized via the [C = O···H–N] intra-hydrogen bond to form the zwitterionic salt instead of the enol form [13]. This intramolecular hydrogen bond effected significantly the C_{ph}-H stretching vibrations to less than 3000 cm^{-1} and C_{Me}-H stretching vibrations 2920–2850 cm^{-1}, The spectrum displays a strong and broad band of the ketone carbonyl at 1713 cm^{-1}, an ester carbonyl band at 1650 cm^{-1}, and an important peak of (C = N) showed at 1562 cm^{-1} [8–10]. Another peak at 1460 cm^{-1} corresponding to (C = C), at 1350 cm^{-1} peak attributed to (C—N), and 1021 cm^{-1} (C—O-C). The band at 1233 cm^{-1} is attributed to C—O stretching vibration and band at 840 cm^{-1} corresponds to C—$H_{aromatic}$ bending vibration [33]. Theoretical DFT/IR calculation revealed the presence of many functional groups composing the compound, and the vibrations of these groups agreed with the values of their experimental counterparts but with significant increase in DFT values. This is not surprising, since the theoretical calculations were performed in the gaseous state, meanwhile, the experimental one was in the solid state, the largest deviation in the wavelength values were detected in C_{ph}-H and C_{Me}-H stretching vibrations with $\Delta_{wavelength}$ = 176–230 cm^{-1}, and the next one was in C = N with $\Delta_{wavelength}$ = 155 cm^{-1} (Fig. 9b). Therefore, the investigation of the comparison between experimental and DFT-IR involved the assessment of R^2 with 0.9981 and RMSD which reflected 107.9854 (Table 3).

3.5. MEP, MO and DOS analysis

The Molecular Electrostatic Potential (MEP) analysis of the desired ligand was performed through DFT calculations using the B3LYP-D3/6–311++*G*(2d,p) method. MEP analysis will provide a piece of useful information about the possibility of molecule-molecule interaction, mainly through H-bonding and nucleophilic functional groups (Fig. S1). The results showed the nucleophilic sites of the N, O, and some C atoms, depicted in red, reflecting their electron richness. The electrophilic sites of hydrogen and some C atoms, depicted in blue, reflected their electron poverty (Fig. S2). These findings suggest the possibility of H-bonding formation in the molecule, consistent with the HSA and XRD results.

The frontier orbitals were represented by the HOMO and LUMO surfaces (Fig. S3) and their energy gap is related to both optical and electrical properties. The calculated ΔE from HOMO/LUMO (0.1725 a.u corresponding to 4.694 eV) and ΔE from HOMO-1/LUMO+1 (0.225 a.u corresponding to 6.120 eV) indicated that the compound is a small soft ligand molecule with ease of electron transfer (Fig. S4). The calculated HOMO/LUMO via ΔE_{DOS} density of state was found to be 4.782 eV (Fig. S4), and the fact that the values of the energies obtained through

Table 3
RMSD calculations for ^{1}H NMR, ^{13}C NMR and FT-IR.

1H NMR				13C NMR				FT-IR			
δ_H(Exp.)	δ_H(DFT)	$\Delta\delta_H$	$(\Delta\delta_H)^2$	δ_c(Exp.)	δ_c(DFT)	$\Delta\delta c$	$(\Delta\delta c)^2$	$W_{no.}$(Exp.)	$W_{no.}$(DFT)	$\Delta W_{no.}$	$(\Delta W_{no.})^2$
1.1	1.2	−0.1	0.01	20.1	21.7	−1.6	2.56	3116	2940	176	30,976
2.1	1.5	0.6	0.36	22.6	26.8	−4.2	17.64	3080	2850	230	52,900
2.3	2.5	−0.2	0.04	24.2	30.3	−6.1	37.21	1815	1705	110	12,100
2.7	2.9	−0.2	0.04	28.7	31.7	−3	9	1716	1650	66	4356
5.7	5.6	0.1	0.01	96.7	101.1	−4.4	19.36	1670	1560	110	12,100
7.1	7.3	−0.2	0.04	107.2	120.6	−13.4	179.56	1635	1480	155	24,025
15.4	13.3	2.1	4.41	124	120.2	3.8	14.44	1400	1350	50	2500
RMSD= 0.8375				129.2	122.6	6.6	43.56	1370	1300	70	4900
				131.8	132.9	−1.1	1.21	1300	1255	45	2025
				144.5	144.2	0.3	0.09	1100	1050	50	2500
				163.2	163	0.2	0.04	1020	1005	15	225
				163.5	168.5	−5	25	950	900	50	2500
				177.1	160.5	16.6	275.56	852	830	22	484
				185.1	182	3.1	9.61				
				RMSD= 5.7026				RMSD= 107.9854			

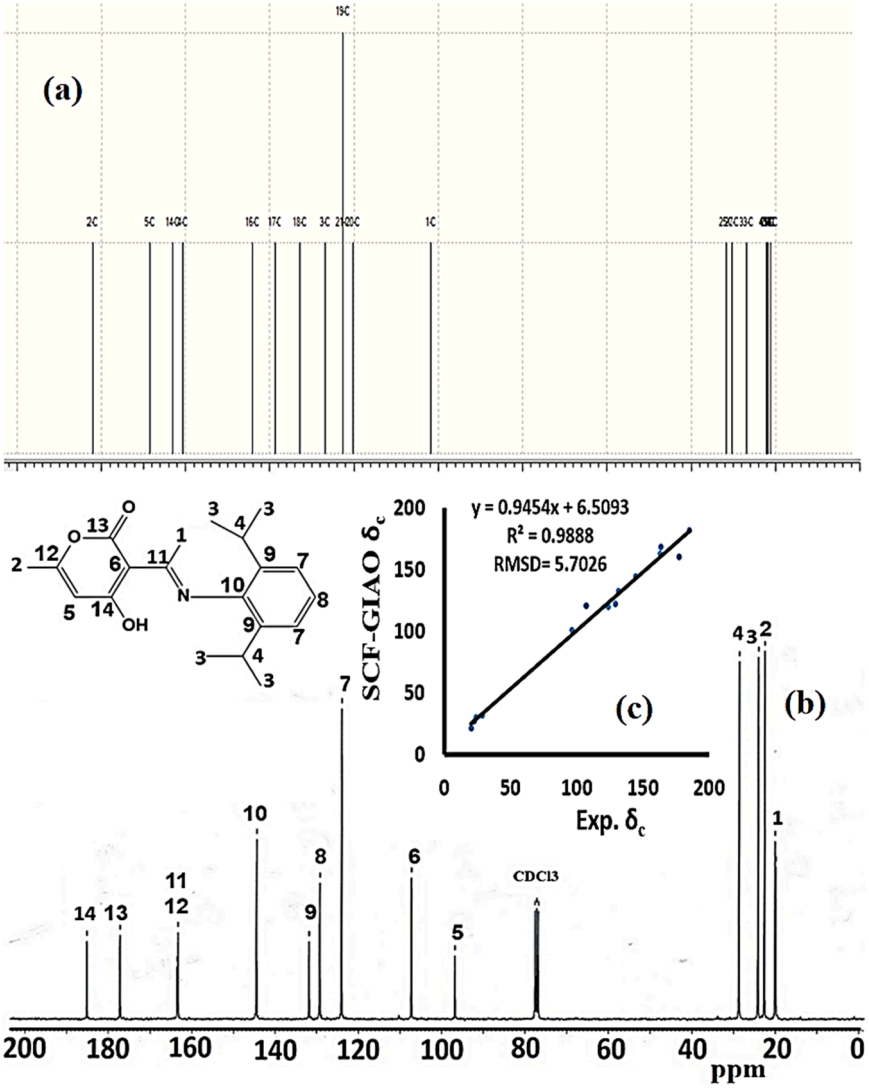

Fig. 8. ^{13}C NMR of the desired ligand: (a)Exp., b) DFT, and (c)Exp/DFT correlation.

both methods were nearly identical with a small deviation of 0.088 eV, making the compound an electronically stable good e-donor and poly-chelate ligand [34].

3.6. *Enol↔imine tautomerization*

Intra-migration single proton tautomerization process is a scientific activity that has recently received attention due to its role in the inter-pretation of genetic mutations and some of the therapeutic activities of organic materials. In this study, to elucidate the hydroxyl proton enol-imine tautomerization mechanism, the relaxed scan was performed for the intramolecular single-proton transfer in a gaseous state using the B3LYP-D3/6–311++*G*(2d-p) level of theory as simplified in Scheme 4. The obtained potential energy surface (PES) and related optimized structures for the two tautomeric forms and the transition state (TS) are given in Fig. 10. It showed that the two tautomeric forms together with the TS are perfectly planar, and there are no appreciable structural changes have been observed in the remaining parts of the molecular structures (Fig. 10). Also, it shows that the keto-Amine form is the highest stable structure with stabilization energy of 19.78 kJ/mol, such seen is in very good coincidence with the structural XRD analysis that reveals the keto-Amine form as the only isolated tautomeric form in the crystalline structure. The PES of intramolecular single-hydrogen shift shows that the TS has an elongated "O–H" bond length from the Enol-Imine tautomer by 0.140 Å [$(O—H)_{Enol\text{-}imine}$ =1.052 Å–$(O—H)_{TS}$ =1.192 Å] and shortened bond length from Keto-Amine form by 0.441 Å [$(O—H)_{Keto\text{-}amine}$ =1.633 Å–$(O—H)_{TS}$ =1.192 Å], while a reverse behavior for the "N–H" bond length is observed; it is shortened from the Enol-Imine form by 0.170 Å [$(N—H)_{Enol\text{-}imine}$ =1.494 Å–$(N—H)_{TS}$ =1.324 Å], and elongated from Keto-Amine form by 0.283 Å [$(N—H)_{Keto\text{-}amine}$ =1.041 Å–$(N—H)_{TS}$ =1.324 Å] as expected for the TS structurer (Fig. 10). Moreover, The PES has shown a very low energy difference for the TS from the Enol-Imine form (ΔE = 3.05 kJ/mol), such find supported that the intramolecular single-proton intra-H-bond migration is the likely mechanism for such tautomerization.

3.7. *TG/DTG thermal and anti-cancer cytotoxicity MTT*

Thermal degradation TG/DTG of the desired ligand was investigated at 25–900 °C temperatures range and 5 °C per minute heating rate, as illustrated in Fig. 11a. The thermal behavior of the desired ligand showed simplicity in the decomposition mechanism, as the compound remained stable to 202 °C and then began to decompose in one step only through a simple broad cracking curve starting from 205 °C and ending at 380 °C with sharp T_{DTG} = 280 °C and ~ zero-gram residue supporting that all the organic content turned into light gases [35] seen in Fig. 11a.

A highly accurate and quick approach for assessing the in vitro anticancer activity of both natural and manufactured compounds is the

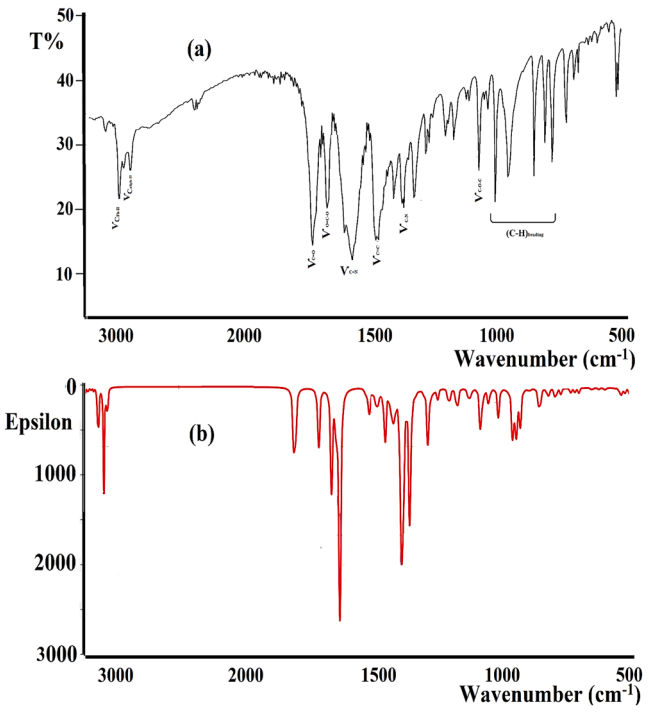

Fig. 9. FT-IR of the desired ligand: (a)Exp., and (b)DFT. .

MTT assay. To compare and assess the product's anticancer efficacy, the intended ligand's activity against HeLa cancer and normal L6 cells was put into practice. HeLa cells have shrunk in the range of 25–40 % with $IC_{50} = 0.055$ μg/ml within the examined concentration range, as shown in Fig. 11b. In general, HeLa cell growth decreased with the rising ligand concentration demonstrating considerable inhibitory actions. Additionally, the substance showed strong activity against normal L6 cells in the range of 49–53 %, although with an IC_{50} <1 μg/ml in the concentration range (Fig. 11b). According to the MTT assay results presented in Fig. 11b, the desired ligand was able to kill cancer cells at extremely low concentrations without harming normal L6 cells. This is a hopeful early indicator for the ligand used in more advanced anticancer assessments in the future work.

4. Conclusion

A good yield of the new zwitterionic Schiff base was achieved during synthesis. The XRD findings corroborated the enol↔imine tautomerization, and other spectral measurements were utilized to determine the preferred structure in solid and liquid phases. Triclinic/P-1, crystal system/space group with $a = 8.3759(18)$ Å, $b = 9.9587(16)$ Å, $c = 11.469(2)$ Å and $\alpha = 79.078(11)^\circ$, $\beta = 86.822(13)^\circ$ and $\gamma = 77.396(11)^\circ$ unit cell dimensions have been reported by SC-XRD. The ligand's backbone contains O and N heteroatoms, which result in different molecular interactions, including the formation of a [N^+—H....^-O] zwitterionic salt intermediate. This has been verified using XRD/HSA and MEP/MAC/NBA analysis. The presence of a zwitterionic salt intermediate as the preferred isomer in the solid-state during enol↔imine tautomerism was also proven through the use of DFT analysis. The

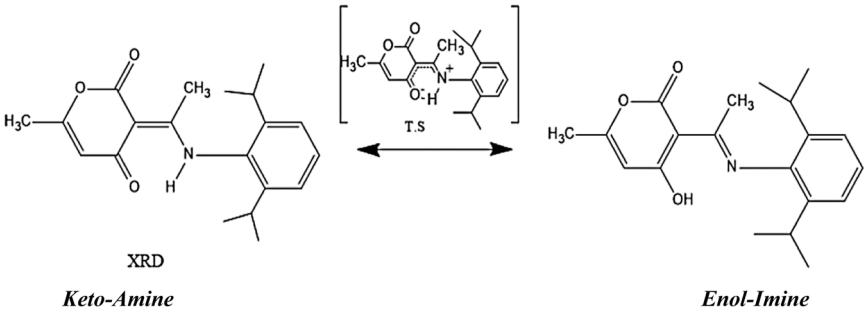

Scheme 4. Enol↔imine tautomerism.

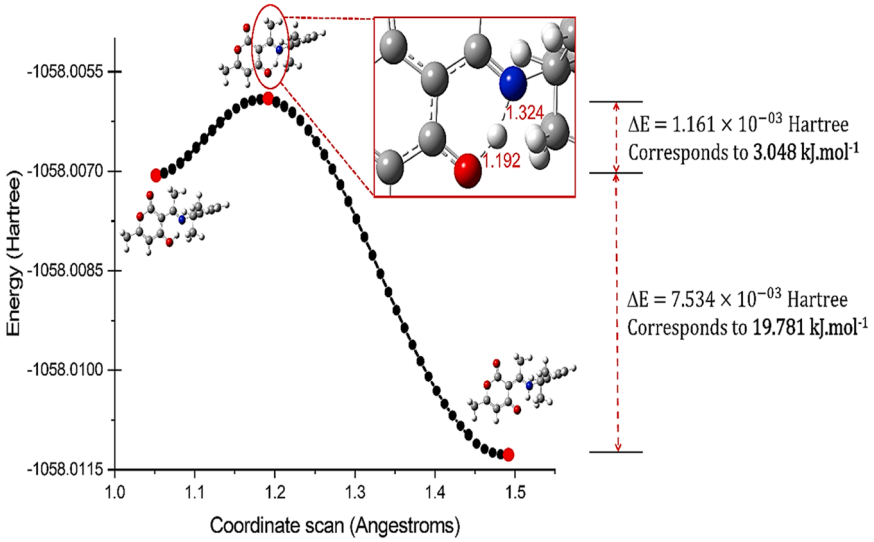

Fig. 10. Gaseous-state DFT enol↔imine tautomerism structures and their energy profiles.

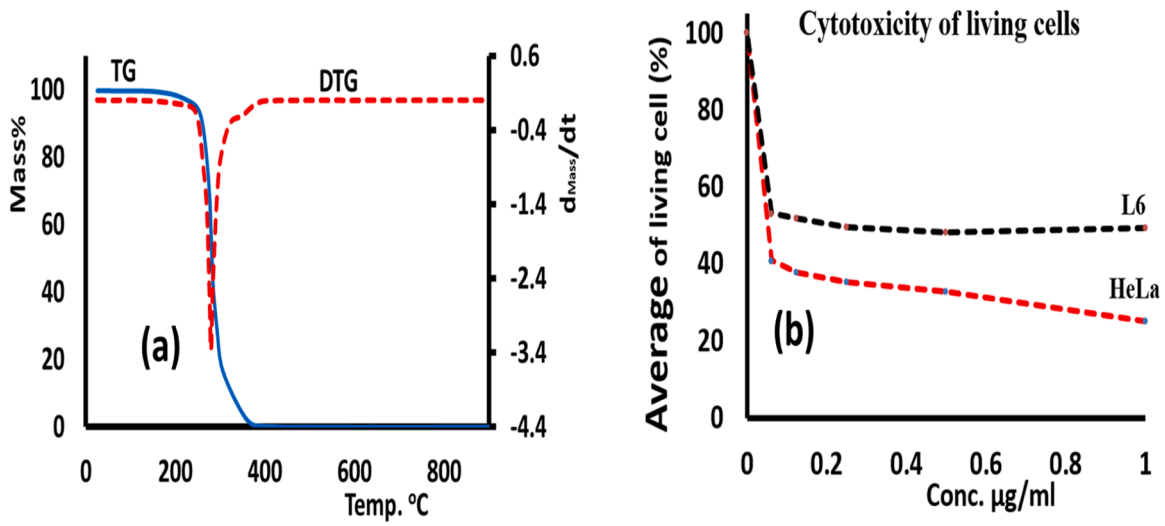

Fig. 11. (a) TG and DTG curves, and (b) Cytotoxicity of HeLa and L6 normal cells using 1 µg/ml, 0.5 µg/ml, 0.25 µg/ml, 0.125 µg/ml, 0.0625 µg/ml concentrations.

desired ligand demonstrated sufficient thermal stability and passed through a simple one-step degradation process. At low doses, the ligand had significant efficacy and specificity against malignant HeLa cells, as seen by an IC50 value of 0.055 µg/ml. However, it did not have any effect on normal L6 cells, as indicated by an IC50 value of <1 g/ml.

Supplementary Information

CCDC no. **2,336,259** contains the supplementary crystallographic data (CIF and HKL file) for SB. These data can be obtained free of charge *via* http://www.ccdc.cam.ac.uk/conts/retrieving.html, or from the Cambridge Crystallographic Data Centre, 12 Union Road, Cambridge CB2 1EZ, UK; fax: (+44) 1223–336–033; or e-mail: deposit@ccdc.cam.ac.uk.

CRediT authorship contribution statement

Salima Tabti: Conceptualization. **Djouhra Aggoun:** Data curation. **Diaa Aref:** Formal analysis. **Ashraf Sawafta:** Data curation. **Amel Djedouani:** Software, Data curation. **Ahmed Abu-Rayyan:** Formal analysis. **Abeer AlObaid:** Software. **Jerome Lhoste:** Resources, Project administration. **Carine Robert:** Software, Project administration. **Sandy Augste:** Supervision, Project administration. **Khalil Shalalin:** Visualization. **Ismail Warad:** Writing – review & editing.

Declaration of competing interest

The authors declare that they have no known competing financial interests or personal relationships that could have appeared to influence the work reported in this paper.

Data availability

Data will be made available on request.

Acknowledgements

The authors thank the Algerian Ministry of Higher Education and Scientific Research (MESRS) and the Directorate General of Scientific Research and Technological Development (DGRSDT) for their financial support. We would like to extend our appreciation to the platforms "Diffusion and Diffraction of X Ray of IMMM" Mans University. The authors extend also their appreciation to the Researchers Supporting Project number (RSP2024R381), King Saud University, Riyadh, Saudi Arabia.

Supplementary materials

Supplementary material associated with this article can be found, in the online version, at doi:10.1016/j.molstruc.2024.138258.

References

[1] S. Mukherjee, J.W. Yang, S. Hoffmann, B. List, Asymmetric enamine catalysis, Chem. Rev. 107 (2007) 5471, https://doi.org/10.1021/cr0684016.
[2] N. Tarannum, M. Singh, Synthesis and characterization of zwitterionic organogels based on Schiff base chemistry, J. Appl. Polym. Sci. 118 (2010) 2821, https://doi.org/10.1002/app.32393.
[3] A.B. El-Meligy, S.H. El-Demerdash, M.A. Abdel-Rahman, M.A. Mahmoud, T. Taketsugu, A.M. El-Nahas, Structures, Energetics, and Spectra of (NH) and (OH) Tautomers of 2-(2-Hydroxyphenyl)-1-azaazulene: A Density Functional Theory/Time-Dependent Density Functional Theory Study, ACS Omega 7 (2022) 14222, https://doi.org/10.1021/acsomega.2c00866.
[4] J.A. Vila, Y.A. Arnautova, Y. Vorobjev, H.A. Scheraga, Assessing the Fractions of Tautomeric Forms of the Imidazole Ring of Histidine in Proteins as a Function of PH, Proc. Natl. Acad. Sci. U.S.A. 108 (2011) 5602, https://doi.org/10.1073/pnas.110237310.
[5] V.I. Minkin, L.P. Olekhnovich, Y.A. Zhdanov, Molecular Design of Tautomeric Compounds, Acc. Chem. Res. 3 (1981) 210, https://doi.org/10.1021/ar00067a003.
[6] N. Özdemir, R. Kağıt, O. Dayan, Investigation of enol-imine/keto-amine tautomerism in (E)-4-[(2-hydroxybenzylidene) amino] phenyl benzenesulphonate by experimental and molecular modeling methods, Mol. Phys. 114 (2016) 757, https://doi.org/10.1080/00268976.2015.1116715.
[7] M. Oda, A. Sugiyama, R. Takeuchi, Y. Fujiwara, R. Miyatake, T. Abe, S. Kuroda, Synthesis, molecular structure, and properties of 2-(2-Hydroxyphenyl)-1-azaazulene, Eur. J. Org. Chem. 6 (2012) 2231, https://doi.org/10.1002/ejoc.201101831.
[8] S. Chetioui, A. Djedouani, Z. Fellahi, J-Pierre Djukic, Christian G. Bochet, A. Zarrouk, I. Warad, Diazene<=>hydrazine tautomerization in MeOH, single proton intra-migration, XRD/HSA-interactions, spectral, optical and DFT/TD-DFT of new hydrazine, J. Mol. Struct. 229 (2021) 129604, https://doi.org/10.1016/j.molstruc.2022.134113.
[9] A. Guerraoui, A. Djedouani, E. Jeanneau, A. Boumaza, A. Alsalme, A. Zarrouk, K.S. M. Salih, I. Warad, Crystal structure and spectral of new hydrazine-pyran-dione derivative: DFT enol↔hydrazone tautomerization via zwitterionic intermediate, hirshfeld analysis and optical activity studies, J. Mol. Struct. 1220 (2020) 128728, https://doi.org/10.1016/j.molstruc.2020.128728.
[10] I. Warad, A.F. Eftaiha, M.A. Al-Nuri, A.I. Husein, M. Assal, A. Abu-Obaid, N. Al-Zaqri, T. Ben Hadda, B. Hammouti, Metal ions as antitumor complexes-Review, J. Mater. Environ. Sci. 4 (2013) 542. http://www.jmaterenvironsci.com/Journal/vol4-4.html.
[11] I. Warad, A.A. Khan, M. Azam, S.I. Al-Resayes, S.F. Haddad, Design and structural studies of diimine/CdX2 (X= Cl, I) complexes based on 2, 2-dimethyl-1, 3-diaminopropane ligand, J. Mol. Struct. 1062 (2014) 167, https://doi.org/10.1016/j.molstruc.2014.01.001.
[12] M. Azam, Z. Hussain, I. Warad, S. Al-Resayes, S.M. Khan, M. Shakir, A. Trzesowska-Kruszynska, R. Kruszynski, Novel Pd(ii)-salen complexes showing high in vitro

anti-proliferative effects against human hepatoma cancer by modulating specific regulatory genes, Dalton Transactions 41 (2012) 10854–1086421, https://doi.org/10.1039/c2dt31143g.
[13] A. Mili, S. Chetioui, A. Djedouani, J.P. Djukic, A. Al Obaid A. Zarroukh I. Warad, Tautomerization of diazene<=>hydrazine via single proton tautomerization, spectral, XRD/HSA-interactions, optical and DFT/TD-DFT of new hydrazine ligand, J. Mol. Struct. 1272 (2023) 134113, https://doi.org/10.1016/j.molstruc.2022.134113.
[14] M.J. Frisch, G.W. Trucks, H.B. Schlegel, G.E. Scuseria, et al., Gaussian 09 W, Gaussian Inc., Wallingford CT, 2009.
[15] S.K. Wolff, D.J. Grimwood, J.J. McKinnon, M.J. Turner, D. Jayatilaka, M. A. Spackman, Crystal Explorer 3.0, University of Western Australia, Perth, 2012.
[16] A.P.E.X.2. Bruker, Bruker SAINT, AXS Inc, 2007. Madison, Wisconsin, USA.
[17] M.C. Burla, R. Caliandro, M. Camalli, B. Carrozzini, G.L. Cascarano, L. DeCaro, C. Giacovazzo, G. Polidori, R. Spagna, SIR2004: an improved tool for crystal structure determination and refinement, J. Appl. Crystallogr. 38 (2005) 381, https://doi.org/10.1107/S002188980403225X.
[18] L.J. Farrugia, WinGX and ORTEP for Windows: an update, J. Appl. Cryst. 45 (2012) 849, https://doi.org/10.1107/S0021889812029111.
[19] G.M. Sheldrick, A short history of SHELX, Acta Crystallogr. Sect A64 (2008) 112, https://doi.org/10.1107/S0108767307043930.
[20] A. Djedouani, S. Boufas, M. Allain, G. Bouet, M. Khan, Zwitterionic 6-methyl-2-oxo-3-[1-(ureidoiminio)ethyl]-2H-pyran-4-olatemonohydrate, Acta Cryst. E71 (2008) 1785, https://doi.org/10.1107/S1600536808026032/wk2091sup0.html.
[21] G. Wojciechowski, M. Ratajczak-Sitarz, A. Katrusiak, W. Schiff, P. Przybylski, B. Brzezinski, Crystal structure of Schiff base derivative of 2,2′-dihydroxybiphenyl-3-carbaldehyde with n-butylamine, J. Mol. Struct. 650 (2003) 191, https://doi.org/10.1016/S0022-2860(03)00159-5.
[22] C.R. Girija, N.S. Begum, 1-Dimethylamino-3-dimethyliminio-2-(p-methoxyphenyl) prop-1-ene perchlorate, Acta Cryst. E60 (2004) o535, https://doi.org/10.1107/S1600536804004593.
[23] C.R. Girija, N.S. Begum, M.A. Sridhar, N.K. Lokanath, J.S. Prasad, 1-Dimethylamino-3-dimethylimino-1-phenylprop-1-ene perchlorate, Acta Cryst. E60 (2004) o586, https://doi.org/10.1107/S1600536804005173.
[24] A. Salhin, A.R. Norfarhah, I.A. Rahman, 1-[(Bromomethyl)(phenyl)methylene]-2-(2,4-dinitro-phenyl)hydrazine, Acta Cryst. E65 (2009) o1221, https://doi.org/10.1107/S1600536809016225/at2763Isup2.hkl.
[25] B.T. Gowda, S. Foro, H. Fuess, N-(4-Chlorophenyl)acetamide, Acta Cryst. E63 (2007) o3392, https://doi.org/10.1107/S1600536809032139.
[26] F.H. Allen, O. Kennard, D.G. Watson, L. Brammer, A.G. Orpen, R. Taylor, Tables of bond lengths determined by X-ray and neutron diffraction. Part 1. Bond lengths in organic compounds, J. Chem. Soc. Perkin Trans. 2 (1987) S1, https://doi.org/10.1039/P298700000S1.
[27] I. Badran, S. Tighadouini, S. Radi, A. Zarrouk, I. Warad, Experimental and first-principles study of a new hydrazine derivative for DSSC applications, J. Mol. Struct. 1229 (2021) 129799, https://doi.org/10.1016/j.molstruc.2020.129799.
[28] I. Warad, S. Musameh, I. Badran, N.N. Nassar, P. Brandao, C.J. Tavares, A. Barakat, Synthesis, solvatochromism and crystal structure of trans-[$Cu(Et_2NCH_2CH_2NH_2)_2$.H_2O]$(NO_3)_2$ complex: Experimental with DFT combination, J. Mol. Struct. 1148 (2017) 328, https://doi.org/10.1016/j.molstruc.2017.07.067.
[29] F. Abu Saleemh, S. Musameh, A. Sawafta, P. Brandao, C.J. Tavares, S. Ferdov, A. Barakat, A. Al Ali, M. Al-Noaimi, I. Warad, Diethylenetriamine/diamines/copper (II) complexes [Cu(dien)(NN)]Br_2: Synthesis, solvatochromism, thermal, electrochemistry, single crystal, Hirshfeld surface analysis and antibacterial activity, Arab. J. Chem. 10 (2017) 845, https://doi.org/10.1016/j.arabjc.2016.10.008.
[30] O. Tamer, N. Dege, G. Demirtas, D. Avcı, Y. Atalay, M. Macit, S. Sahin, Crystal structure and spectroscopic characterization of (E)-2-(((4-bromo-2-(trifluoromethoxy)phenyl)imino)methyl)-4-nitrophenol: A combined experimental and computational study, J. Mol. Struct. 1063 (2014) 295–306, https://doi.org/10.1016/j.molstruc.2014.01.079.
[31] M.R. Albayati, S. Kansız, N. Dege, S. Kaya, R. Marzouki, H. Lgaz, R. Salghi, I.H. Ali, M.M. Alghamdi, I.M. Chung, Synthesis, crystal structure, Hirshfeld surface analysis and DFT calculations of 2-[(2,3-dimethylphenyl)amino]-N'-[(E)-thiophen-2-ylmethylidene]benzohydrazide, J. Mol. Struct. 1205 (2020) 127654–127664, https://doi.org/10.1016/j.molstruc.2019.127654.
[32] N. Dege, N.S. Enyüz, H. Batın, N. Günay, D. Avcı, O. Tamer, Y. Atalay, The synthesis, characterization and theoretical study on nicotinic acid [1-(2,3-dihydroxyphenyl)methylidene]-hydrazide, Spectrochim. Acta A Mol. Biomol. Spectrosc. 120 (2014) 323–331, https://doi.org/10.1016/j.saa.2013.10.030.
[33] N. Goswami, H.P. Gogoi, Barman A hydrazine-based unsymmetrical bis-imine-Schiff base as a chemosensor for turn-off fluorescence and naked-eye detection of Cu^{2+} ion: Application in aqueous media using test strips, J. Photochem. Photobiol. A Chem. 446 (2024) 115106, https://doi.org/10.1016/j.jphotochem.2023.115106.
[34] Y. Hijji, R. Rajan, H.B. Yahia, S. Mansour, A. Zarrouk, I. Warad, One-pot microwave-assisted synthesis of water-soluble pyran-2,4,5-triol glucose amine Schiff base derivative: XRD/HSA interactions, crystal structure, spectral, thermal and a DFT/TD-DFT, Crystals 11 (2021) 117–131, https://doi.org/10.3390/cryst11020117.
[35] S. Demir, F. Tinmaz, N. Dege, I. Ilhan, Vibrational spectroscopic studies, NMR, HOMO–LUMO, NLO and NBO analysis of 1-(2-nitrobenzoyl)-3,5-diphenyl-4,5-dihydro-1H-pyrazole with use X-ray diffractions and DFT calculations, J. Mol. Struct. 1108 (2016) 637–648, https://doi.org/10.1016/j.molstruc.2015.12.057.